MDPI

Article

Research on Degradation State Recognition of Axial Piston Pump under Variable Rotating Speed

Rui Guo [1,2,3,*] , Yingtang Liu [1], Zhiqian Zhao [1], Jingyi Zhao [1,3] , Jianwei Wang [1,4] and Wei Cai [1,4]

1   Hebei Provincial Key Laboratory of Heavy Machinery Fluid Power Transmission and Control, Yanshan University, Qinhuangdao 066004, China; lyt1997@stumail.ysu.edu.cn (Y.L.); zzq623310996@163.com (Z.Z.); zjy@ysu.edu.cn (J.Z.); wangjianwei@ysu.edu.cn (J.W.); caiwei@ysu.edu.cn (W.C.)
2   Key Laboratory of Space Launching Site Reliability Technology, Xichang Satellite Launch Center, Haikou 571126, China
3   Hebei Key Laboratory of Special Delivery Equipment, Yanshan University, Qinhuangdao 066004, China
4   Key Laboratory of Advanced Forging & Stamping Technology and Science, Yanshan University, Qinhuangdao 066004, China
*   Correspondence: guorui@ysu.edu.cn

Abstract: Under the condition of variable rotating speed, it is difficult to extract the degradation characteristics of the axial piston pump, which also reduces the accuracy of degradation recognition. To address these problems, this paper proposes a degradation state recognition method for axial piston pumps by combining spline-kernelled chirplet transform (SCT), adaptive chirp mode pursuit (ACMP), and extreme gradient boosting (XGBoost). Firstly, SCT and ACMP are proposed to deal with the vibration signal instability and high noise of the axial piston pump under variable rotating speed. The instantaneous frequency (IF) of the axial piston pump can be extracted effectively by obtaining the accurate time-frequency distribution of signal components. Then, stable angular domain vibration signals are obtained by re-sampling, and multi-dimensional degradation characteristics are extracted from the angular domain and order spectrum. Finally, XGBoost is used to classify the selected characteristics to recognize the degradation state. In this paper, the vibration signals in four different degradation states are collected and analyzed through the wear test of the valve plate of the axial piston pump. Compared with different pattern recognition algorithms, it is verified that this method can ensure high recognition accuracy.

Keywords: axial piston pump; variable rotating speed; degradation state recognition; SCT; ACMP; XGBoost

1. Introduction

Axial piston pumps have been applied widely in aerospace, robots, construction machinery, and other fields because of their advantages of high integration, diverse control modes, and a wide regulating range of rotating speed and load [1]. As the power element of the hydraulic system, the performance of the axial piston pump directly affects whether the whole hydraulic system can work normally [2]. Therefore, identifying the degradation state of the axial piston pump in time can not only bring great convenience to the maintenance of the hydraulic system, but also improve the reliability and safety of the hydraulic system [3].

However, at present, research on the degradation state recognition of the piston pump is mostly based on the assumption of constant rotating speed, while studies on the degradation recognition of piston pumps under variable rotating speed are not in-depth. Under the condition of variable rotating speed, the vibration signal is non-stationary and the statistical characteristics change with time [4–6], so the common signal processing methods such as Fourier transform [7] and band-pass filtering are no longer applicable. Therefore, how to obtain accurate equipment-related state characteristics at variable rotating speeds

has become a hot topic in the research of state recognition and fault diagnosis of rotating machinery in recent years [8–11].

To reduce the impact of speed change on signal feature extraction, scholars have done a lot of research and analysis. Liu et al. [12] obtained the frequency spectrum of the rolling bearing sound signal by short-time Fourier transform (STFT) [13], and then automatically extracted fault features by using sparse autoencoder techniques; Wang et al. [14] estimated the instantaneous frequency of a variable speed planetary piston pump by nonlinear STFT, and obtained the corresponding phase curve; Goharrizi et al. [15] determined the health threshold by performing a discrete wavelet transform on the pressure signal of the hydraulic actuator to extract the characteristic parameters of the health state of the hydraulic actuator; Wu et al. [16] used continuous wavelet transform (CWT) and time-frequency analysis to diagnose the fault of variable rotating speed piston pump; Khadem et al. [17] applied the multi-wavelet transform to the fault diagnosis of the piston pump, and the test results show that it could better fulfill the extraction of pulse characteristics.

The solutions proposed by the above scholars are health state feature extraction methods based on time-frequency analysis, which is mainly represented by STFT and wavelet transform (WT), and their core idea is to analyze the relationship between rotational speed and signal through data. Due to its simplicity and robustness, STFT has been widely applied. However, the efficiency of STFT depends largely on the size and type of the window, so STFT can only be performed for simple signal time-frequency structure analysis [18]; although the WT overcomes the shortcoming that the window of STFT does not change with frequency, the wavelet basis function of WT has no clear benchmark for selection, and different basis functions will lead to different signal analysis results, and there is also energy leakage in the WT due to the filter and the signal frequency band [19].

In the aspect of mechanical fault diagnosis and state recognition, techniques such as support vector machine (SVM) [20,21] and artificial neural network (ANN) [22,23] have been widely accepted. Reference [24] established an incomplete wavelet packet analysis model consisting of five-layer discrete wavelet transform and four-layer wavelet packet analysis, and applied multilayer ANN for engine fault classification and recognition; in reference [25], the state feature information and natural characteristics of signals were dug from several aspects, and the SVM based on particle swarm optimization was used to implement the multi-state recognition of rolling bearings. Meanwhile, it is to be noted that the ANN needs to be trained iteratively, which requires a large amount of calculation, takes a long time, and the results are difficult to explain; SVM needs to generate a kernel matrix, which takes up a lot of space and takes a long time to calculate [26].

Aiming at the above problems, this paper proposes a degradation state recognition method for axial piston pumps based on SCT, ACMP, and XGBoost. Firstly, ACMP is used to complete the decomposition of the corresponding time-domain signal component, and then the relevant instantaneous frequency is extracted by SCT, so that the signal reconstruction in the angle domain and the order analysis of the reconstructed signal are realized. Finally, the classification model is established by selecting the peak value, pulse, kurtosis, and other indexes of the vibration signal of the piston pump degradation test as the degradation characteristics, and then the pattern recognition of the piston pump in different states is realized by XGBoost. By comparing different algorithms, it is verified that this method can ensure high recognition accuracy while reducing computation time.

2. Theoretical Background

2.1. Spline-Kernelled Chirplet Transform (SCT)

To address the shortcomings of energy divergence and ridge line ambiguity in traditional time-frequency analysis methods, the linear chirplet transform (CT) [27] was extended by replacing the linear chirp kernel with a spline function, which was optimized from the perspective of the kernel function, and the correlation principle of SCT [28] was introduced.

SCT extends the performance of traditional CT. It can analyze continuous and non-linear instantaneous frequency signals, iteratively calculate the best fitting spline, find the most suitable frequency rotation operator and frequency shift operator, and accurately complete time-frequency analysis. The SCT of the signal is defined as:

$$SCT(\tau, \omega, Q; \sigma) = \int_{-\infty}^{+\infty} \bar{z}(t) w_\sigma(t - \tau) e^{-j\omega t} dt \qquad (1)$$

with

$$\begin{cases} \bar{z}(t) = z(t)\phi^R(t, Q)\phi^S(t, \tau, Q) \\ \phi^R(t, Q) = \exp(-j\sum_{k=1}^{n} \frac{q_k^i}{k}(t - t_i)^k + \gamma_i) \\ \phi^S(t, \tau, Q) = \exp(j\sum_{k=1}^{n} q_k^i(\tau - t_i)^{k-1}t) \end{cases} \qquad (2)$$

where, $\phi^R(t, Q)$ is the frequency-rotate operator; $\phi^S(t, \tau, Q)$ is the frequency-shift operator; $Q(i, k) = q_k^i$ is the local polynomial coefficient matrix of the spline kernel. γ_i needs to be met:

$$\gamma_i - \gamma_{i+1} = \sum_{k=1}^{n} \frac{q_k^{i+1}}{k}(t_i - t_{i+1})^k \qquad (3)$$

when $i = 1$, $\gamma_i = 0$.

In particular, SCT consists of three sequential operations:

(1) The signal is rotated in the time-frequency plane by increasing the instantaneous frequency of $\phi^R(t, Q)$;
(2) By increasing the frequency of $\phi^S(t, \tau, Q)$ at τ, the signal is shifted in the time-frequency plane;
(3) The signal is processed by short-time Fourier transform (STFT), and the window is w_σ.

Through approximation and convergence of the spline kernel function and rotation and displacement of the arithmetic operator in SCT, the time-frequency distribution with high energy concentration can be generated, and then the accurate instantaneous frequency and the corresponding relationship between instantaneous frequency and rotating speed can be obtained.

2.2. Instantaneous Frequency Estimation Based on Analytic Signal Analysis Method

Traditional instantaneous frequency estimation of analytic signals mainly determines the number of signal patterns in advance based on optimized technology, and then finds all signal patterns. In fact, this method cannot accurately determine the number of patterns of the test signal, and the bandwidth parameter of the traditional method is fixed, which cannot solve the problem of frequency band overlap. The band overlap problem is shown in Figure 1.

To solve the above-mentioned problems, this paper uses ACMP [29] to decompose the signal modes and complete the extraction of instantaneous frequency. ACMP is composed of three main parts: pattern recursion, extraction framework, and bandwidth parameter adaptive adjustment algorithm. ACMP uses the matching pursuit method [30] to recursively decompose and extract the signal patterns one by one. There is no need to input the number of decomposed signals, and the bandwidth parameter can be adaptively updated with the iteration of the algorithm. Moreover, the ACMP algorithm uses the sparse matrix to decompose the signal, which can better shorten the decomposition time of the signal.

ACMP can decompose the following signal models:

$$s(t) = \sum_{i=1}^{k} s_i(t) = \sum_{i=1}^{k} A_i(t) \cos(2\pi \int_0^t f_i(\tau) d\tau + \varphi_i) \qquad (4)$$

where, $s(t)$ is the superposition of k frequency modulated signals $s_i(t)$, $i = 1, 2, 3 \ldots, k$; $A_i(t)$ is the instantaneous amplitude; $f_i(t)$ is the instantaneous frequency; φ_i is the initial phase of the i-th component $s_i(t)$.
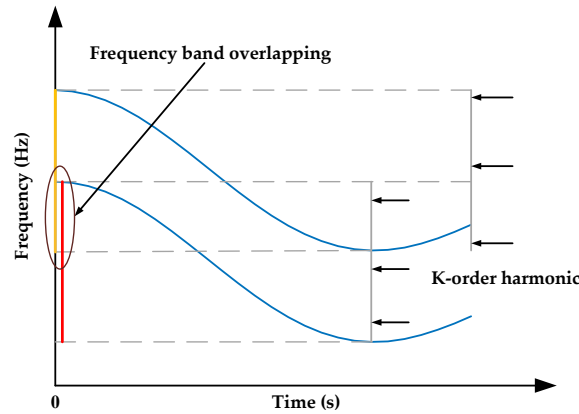

Figure 1. Frequency band overlap.

Due to the stability issues, it is difficult to estimate all modes of the signal simultaneously [31]. ACMP uses a greedy algorithm to estimate signal components and extracts the signal patterns one by one without specifying the format of the patterns in advance. ACMP solves the following problems in extracting the i-th signal pattern:

$$\min_{\{a_i(t), \{\beta_i(t)\}, \hat{f}_i(t)\}} \left\{ \left\| a_i''(t) \right\|_2^2 + \left\| \beta_i''(t) \right\|_2^2 + \gamma \| s(t) - s_i(t) \|_2^2 \right\} \tag{5}$$

with

$$s_i(t) = a_i(t) \cos\left(2\pi \int_0^t \hat{f}_i(\tau) d\tau\right) + \beta_i(t) \sin\left(2\pi \int_0^t \hat{f}_i(\tau) d\tau\right) \tag{6}$$

where γ is the weight coefficient and $\gamma > 0$; $a_i(t)$ and $\beta_i(t)$ are two demodulated signals. $\hat{f}_i(t)$ is a frequency function; the third term of Equation (5) represents the energy of the residual signal, which is a form of a greedy algorithm that makes the residual tend to zero by continuous iteration.

The constraint condition of Equation (6) is brought into Equation (5) and simplified to obtain the following objective function:

$$J_\gamma(u_i, f_i) = \| \Phi u_i \|_2^2 + \gamma \| s - G_i u_i \|_2^2 \tag{7}$$

with

$$\begin{aligned} u_i &= \begin{bmatrix} a_i^T & \beta_i^T \end{bmatrix}^T \\ f_i &= \begin{bmatrix} \hat{f}_i(t_0) \cdots \hat{f}_i(t_{N-1}) \end{bmatrix}^T \\ \Phi &= \begin{bmatrix} P & 0 \\ 0 & P \end{bmatrix} \\ s &= \begin{bmatrix} s(t_0) \cdots s(t_{N-1}) \end{bmatrix}^T; \\ G_i &= \begin{bmatrix} C_i & D_i \end{bmatrix} \end{aligned} \tag{8}$$

with

$$\begin{aligned} a_i &= \begin{bmatrix} a(t_0) \cdots a(t_{N-1}) \end{bmatrix}^T \\ \beta_i &= \begin{bmatrix} \beta(t_0) \cdots \beta(t_{N-1}) \end{bmatrix}^T \\ C_i &= diag[\cos \phi_i(t_0) \cdots \cos \phi_i(t_{N-1})] \\ D_i &= diag[\sin \phi_i(t_0) \cdots \sin \phi_i(t_{N-1})] \end{aligned} \tag{9}$$

where P is a second-order difference matrix; $\phi_i(t) = 2\pi \int_0^t \hat{f}_i(\tau) d\tau$.

Since the objective function $J_\gamma(u_i, f_i)$ is non-linearly related to the instantaneous frequency, it is difficult to update the instantaneous frequency directly with the $J_\gamma(u_i, f_i)$

gradient. The instantaneous frequency increment can be obtained by arctangent demodulation as:

$$\Delta f_i^n(t) = -\frac{1}{2\pi}\frac{d}{dt}\left(\arctan\left(\frac{\beta_i^n(t)}{a_i^n(t)}\right)\right) \tag{10}$$

where n is the number of iterations.

In addition, to reduce the effect of noise, the instantaneous frequency increment needs to meet the low-pass property. It is not difficult to obtain the display expression of the increment as:

$$f_i^{n+1} = f_i^n + \Delta f_i^n \tag{11}$$

Therefore, the instantaneous frequency can be updated by Equation (11).

Due to the convergence of the ACMP, how to accurately select the initial instantaneous frequency is an important part of improving the signal decomposition and instantaneous frequency extraction. In this paper, the wavelet ridge method is used to extract the ridge with the strongest energy in the time-frequency distribution as the initial instantaneous frequency for the iterative convergence of the ACMP algorithm.

2.3. Order Analysis Method Based on SCT and ACMP

The change in rotational speed will affect the stability of vibration signals, and spectrum ambiguity will appear when the Fourier transform is used directly. In order to solve the spectrum ambiguity problem and avoid large errors in the subsequent analysis, this paper proposes an order analysis method based on SCT and ACMP to complete the signal reconstruction in the angle domain and the order analysis of the reconstructed signal.

The calculation process of this method is shown in Figure 2. Aiming at the vibration signal under variable rotational speed, first, the multi-component signal is decomposed into single-component signals by the ACMP method, so as to obtain the modal component of the k-order signal. Secondly, the SCT method is used for the time-frequency analysis of the k-order signal mode component, and the component ridgeline of the k-order signal is optimized to obtain the accurate time-frequency distribution of the k-order signal component. Then, the accurate k-order instantaneous frequency is extracted from the time-frequency distribution by using the wavelet ridge method. Finally, the reconstructed angle domain stationary signal is obtained by the equal angle resampling method.
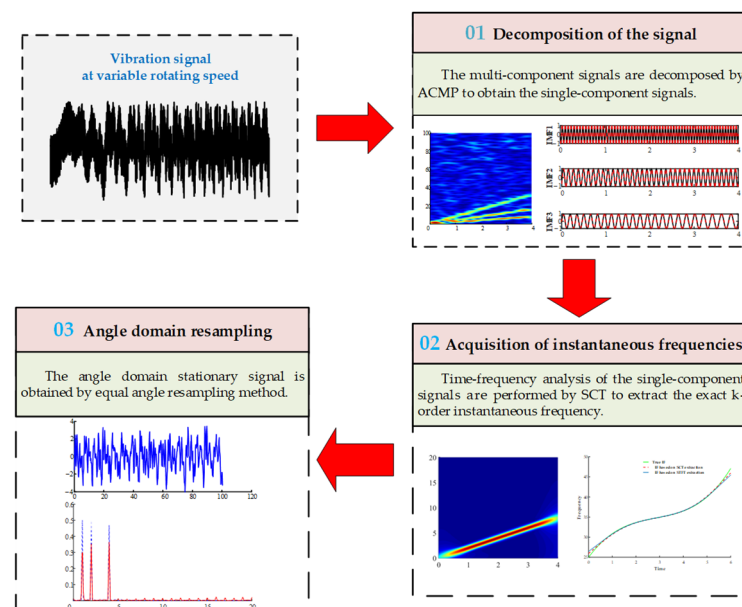

Figure 2. Research process.

2.4. Extreme Gradient Boosting (XGBoost)

To address the problem that traditional tree integration methods are difficult to train data in parallel [32], this paper uses XGBoost for classification, which can intelligently handle missing data and avoid overfitting while processing data in parallel [33]. The XGBoost model is shown below:

$$\hat{y}_i = \sum_{k=1}^{K} f_k(x_i), \ f_k \in F \tag{12}$$

where K is the number of decision trees; $f_k(x_i)$ is a function of the k-th decision tree input x_i of t; $\hat{y}_i$ is the predicted value; F is all possible regression trees sets. The objective function of XGBoost is:

$$X_{obj} = \sum_{i=1}^{n} l(y_i, \hat{y}_i) + \sum_{k=1}^{K} \Omega(f_k) \tag{13}$$

with

$$\Omega(f_k) = \gamma T + \frac{1}{2} \lambda \|w\|^2 \tag{14}$$

where $\sum_{i=1}^{n} l(y_i, \hat{y}_i)$ is the loss function; $\sum_{k=1}^{K} \Omega(f_k)$ is a regularization term; T is the number of leaf nodes; w is the score of leaf nodes; γ is the leaf penalty coefficient; λ ensures that the score of the leave nodes is not too large.

The XGBoost builds a tree with feature parameters, every time a tree (a classified feature node) is added, a new function $f_i(X, \theta_i)$ is learned, and then the final predicted residuals are fitted with the learning results, and finally k trees containing k classification feature nodes are obtained. For the predicted score of each sample, it is necessary to find all the corresponding leaf nodes according to the characteristics of the sample, and the sum of the scores of all leaf nodes is the predicted value of the sample. The principle is shown in Figure 3.
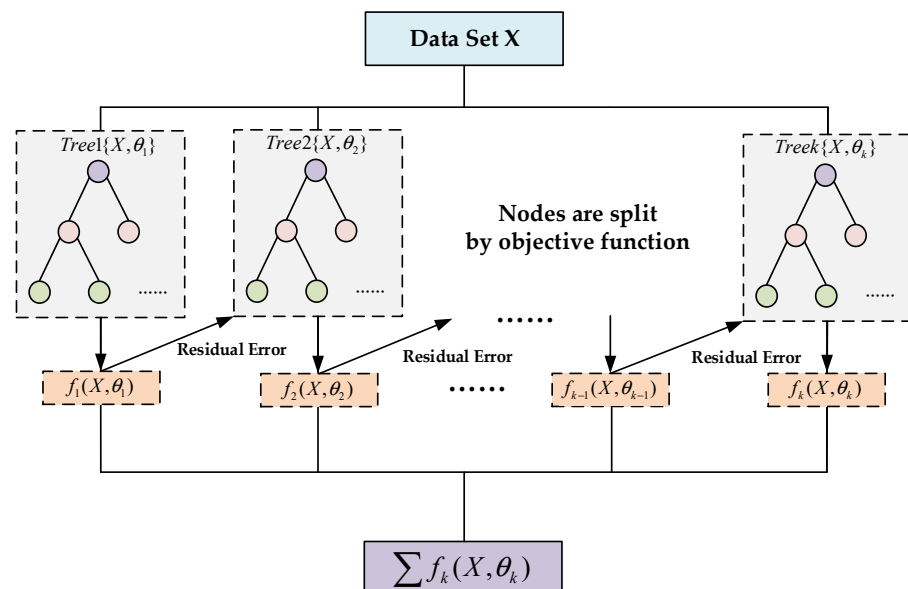

Figure 3. The principle of XGBoost.

3. Piston Pump Degradation Test Verification at Variable Rotating Speed

In this test, different health states of the piston pump are simulated by replacing the valve plate of the piston pump with different wear degrees, so that the vibration, motor speed, and other signals under variable rotating speed conditions can be collected for analysis. Then, the signals are processed using the method proposed in this paper.
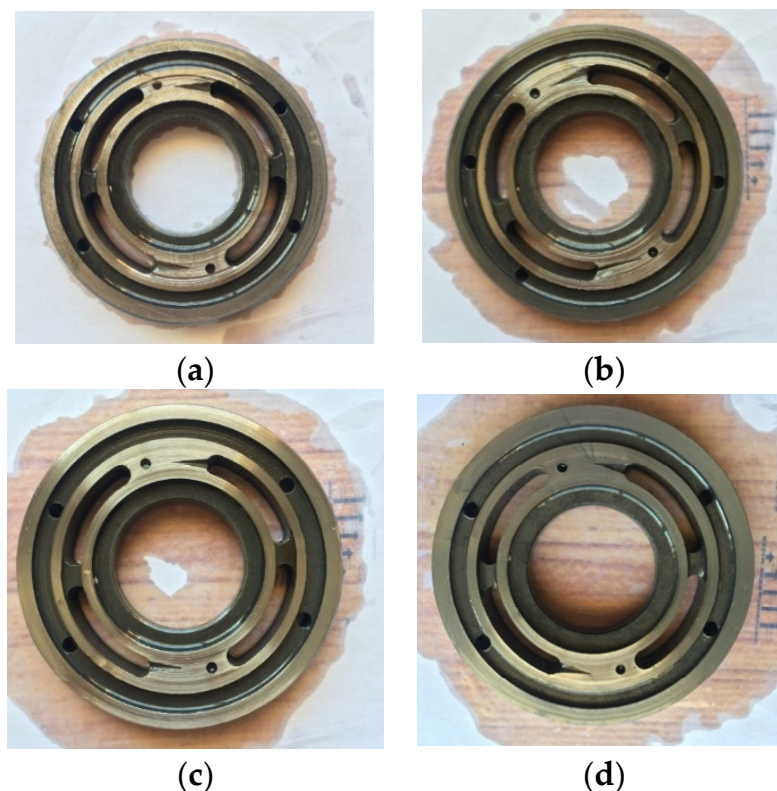
3.1. Design of Degradation Test

In this test, the motor speed is indirectly adjusted by changing the frequency of the frequency converter, and the motor is controlled to complete the linear deceleration. The process is that the frequency is linearly reduced from 50 Hz to 30 Hz for 6 s. The rated speed of the motor is 1500 r/min.

The axial piston pump is selected as the test object in this paper. By artificially manufacturing the wear loss, four states with increasing wear degrees of the piston pump valve plates are simulated. The degrees are: zero wear, mild wear, moderate wear and severe wear. The specific test plan is shown in Table 1.

Table 1. Test plan.

Wear States	Wear Loss	Rotational Speed Variation	Test Pressure (MPa)
zero wear	0 mm	deceleration	10
mild wear	0.0432 mm	deceleration	10
moderate wear	0.1248 mm	deceleration	10
severe wear	0.4661 mm	deceleration	10

The valve plates for the test are shown in Figure 4.

(a)

(b)

(c)

(d)

Figure 4. Valve plates under different wear states: (**a**) Zero wear; (**b**) Mild wear; (**c**) Moderate wear; (**d**) Severe wear.

3.2. Establishment of Degradation Test Bench

Figure 5 is the on-site physical picture of the piston pump degradation test bench, and its system schematic diagram is shown in Figure 6. The swashplate axial piston pump is selected as the tested pump, and its detailed parameters are shown in Table 2.
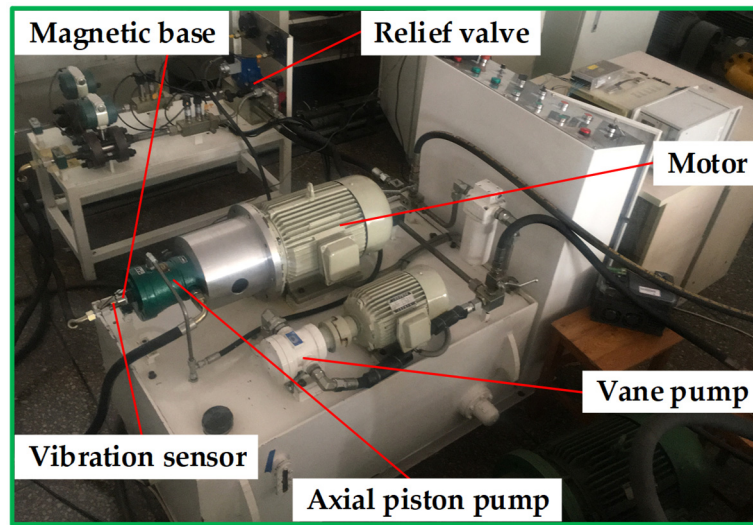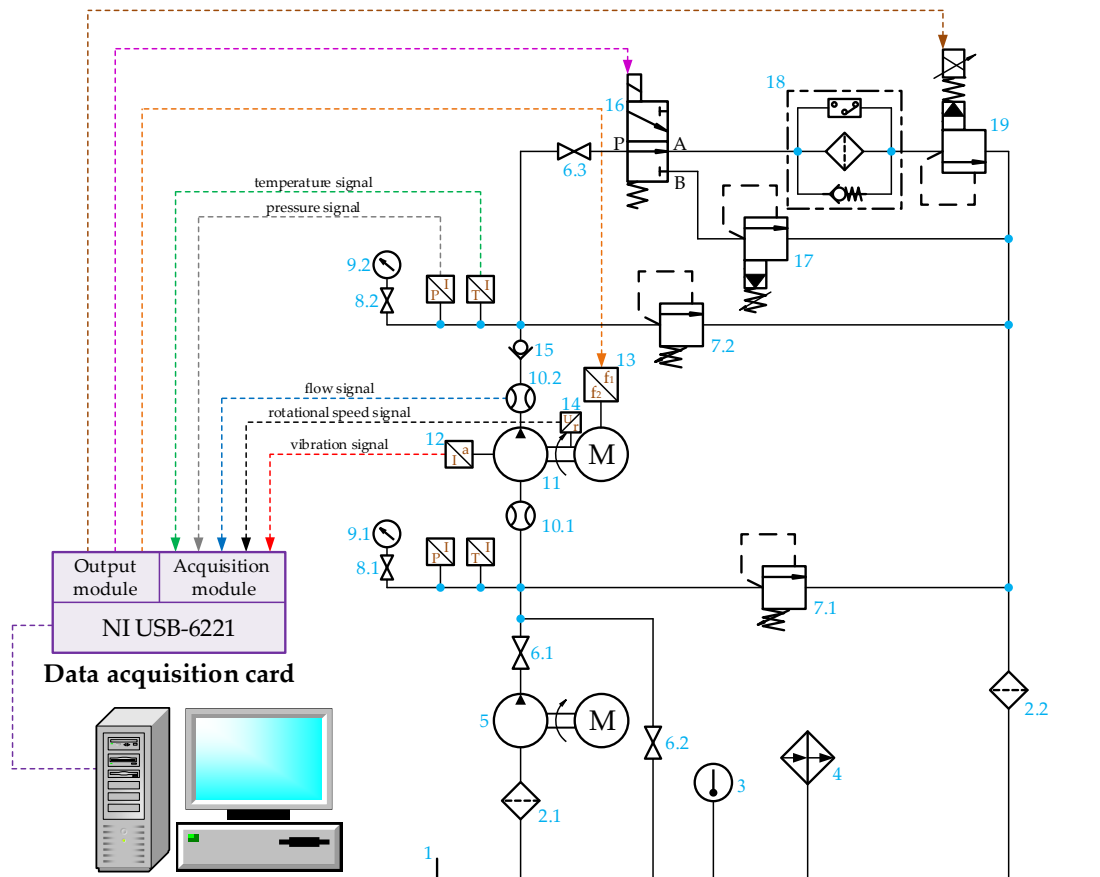
Figure 5. Degradation test bench of axial piston pump.

1—tank   2—filter   3—liquid thermometer   4—thermoregulator
5—vane pump   6—stop valve   7—direct relief valve   8—switch valve
9—pressure meter   10—flowmeter   11—axial piston pump   12—vibration sensor
13—frequency converter   14—tachometer   15—check valve
16—electromagnetic directional valve   17—pilot relief valve
18—high pressure filter   19—electro-proportional relief valve

Figure 6. System schematic diagram for the degradation test of axial piston pump.

Table 2. Basic parameters of piston pump.

Model Number	Number of Pistons	Theoretical Displacement	Rated Pressure
10MCY14-1B	7	10 mL/r	31.5 MPa

In this test, the frequency converter was used to adjust the motor speed. In order to stabilize the pressure of the hydraulic system when replacing the valve plate with different degrees of wear, a vane pump was installed in the system as the charge pump to maintain the system's pressure stability, and the pressure of the hydraulic system circuit was controlled by adjusting the opening size of the pilot relief valve. Meanwhile, to minimize the interference of background noise, we use the magnetic base to install a vibration sensor on the tested piston pump shell parallel to the valve plate.

First of all, during the experiment, we installed a wear-free valve plate on the piston pump under test, adjusted the pilot relief valve to stabilize the system pressure at 10 MPa, and adjusted the potentiometer to change the parameters of the frequency converter, so that the motor speed linearly decreased from 1500 r/min to 900 r/min, lasting for 6 s. At the same time, we set the sampling frequency of the signal acquisition system to 20 khz and the sampling time to 6 s. Finally, the LabVIEW control program was run to collect signals. After collecting this set of signals, the valve plates in other worn states were replaced in turn, the experiment was repeated, and the next set of signals was collected.

3.3. Data Analysis of Axial Piston Pump

The vibration signals of the piston pump under four different states are shown in Figure 7. To reduce the test error and calculation time, the first four seconds of the signal are selected for analysis. With the continuous increase of wear, the amplitude of each state signal is also gradually increasing. In this test, the rotational speed is a decreasing process, and the amplitude energy of the signal along the time axis is also gradually decreasing.
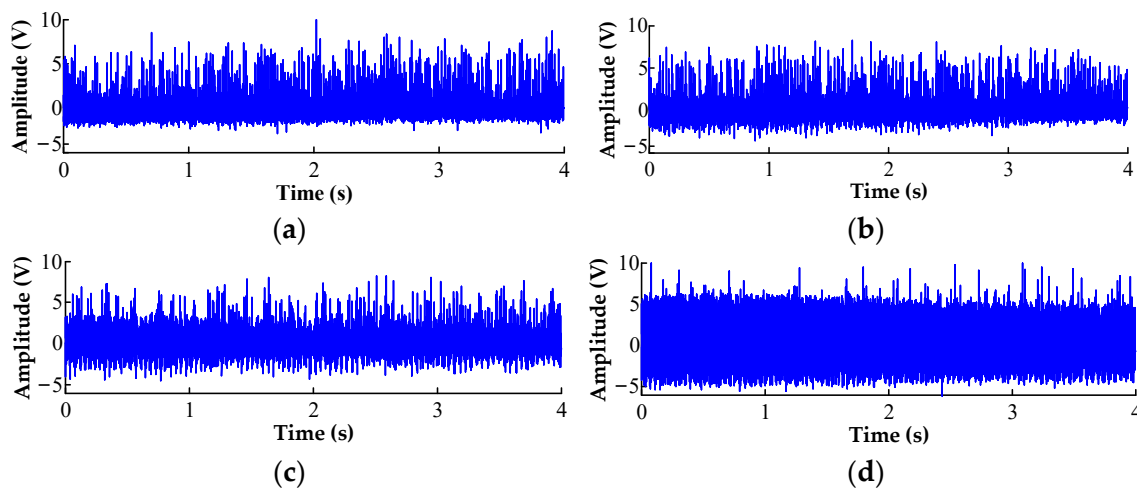
Figure 7. Vibration signals of different wear states: (**a**) Zero wear; (**b**) Mild wear; (**c**) Moderate wear; (**d**) Severe wear.

Taking the vibration signal of the variable rotating speed piston pump under severe wear as an example, it is found that the frequency ambiguity is serious through Fourier transform on the vibration signal, as shown in Figure 8. Therefore, the traditional spectrum analysis methods cannot be directly used to find the degradation characteristics of the piston pump. The fundamental frequency of the piston pump rotating speed is about 25 Hz, as the selected axial piston pump is a 7-piston type, so its piston fundamental frequency should be about 175 Hz.
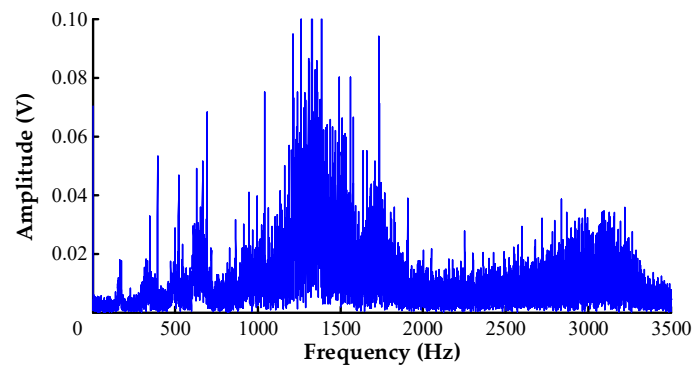
Figure 8. Signal spectrogram diagram under severe wear state.

The time-frequency diagram under severe wear condition is obtained by STFT. The k-order signal component is obtained by ACMP, and the accurate instantaneous frequency is obtained by SCT. The results are shown in Figure 9.

(**a**)   (**b**)
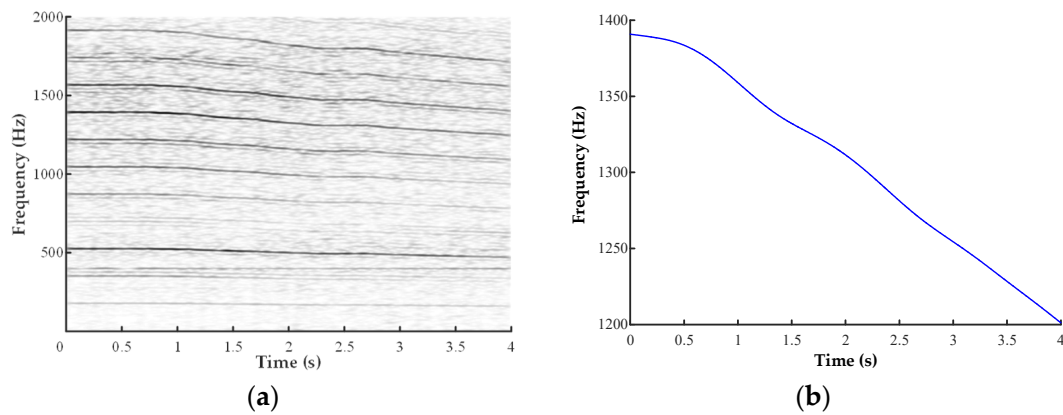
Figure 9. (**a**) Time-frequency diagram based on STFT; (**b**) Instantaneous frequency based on SCT and ACMP.

In this paper, the instantaneous frequency of the k-order harmonic is obtained by obtaining the highest energy signal component, and then the angular domain vibration signal is obtained according to the order algorithm; see Figure 10a below. Through the order analysis of the obtained angular vibration signal, the order spectrum is obtained, as shown in Figure 10b. It can be seen from Figure 10b that the order distribution is clear and the frequency ambiguity caused by the speed change is solved. There are obvious peaks at the integral multiple of order 7 and order 7, and the sideband near the natural frequency is obvious, which is caused by local wear of the valve plate.

(**a**)   (**b**)
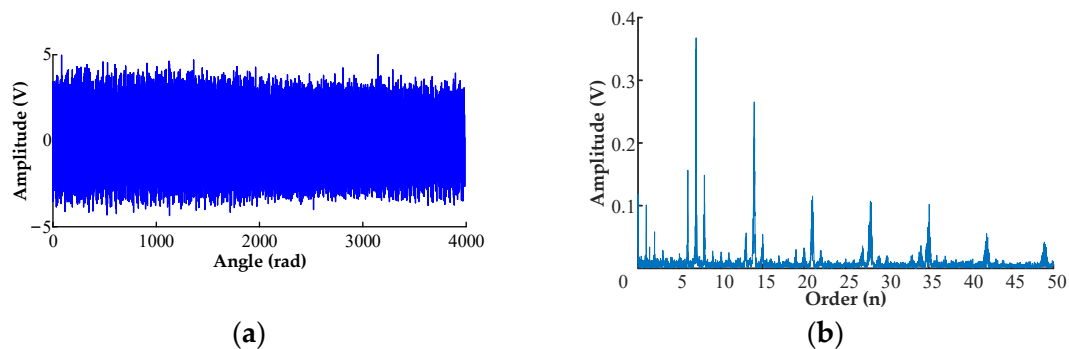
Figure 10. (**a**) Angular domain vibration signal in severe wear state; (**b**) Order spectrogram in severe wear state.

The angular domain signal reconstruction and order analysis under different degradation states are completed by the above method, and the results are shown in Figure 11.
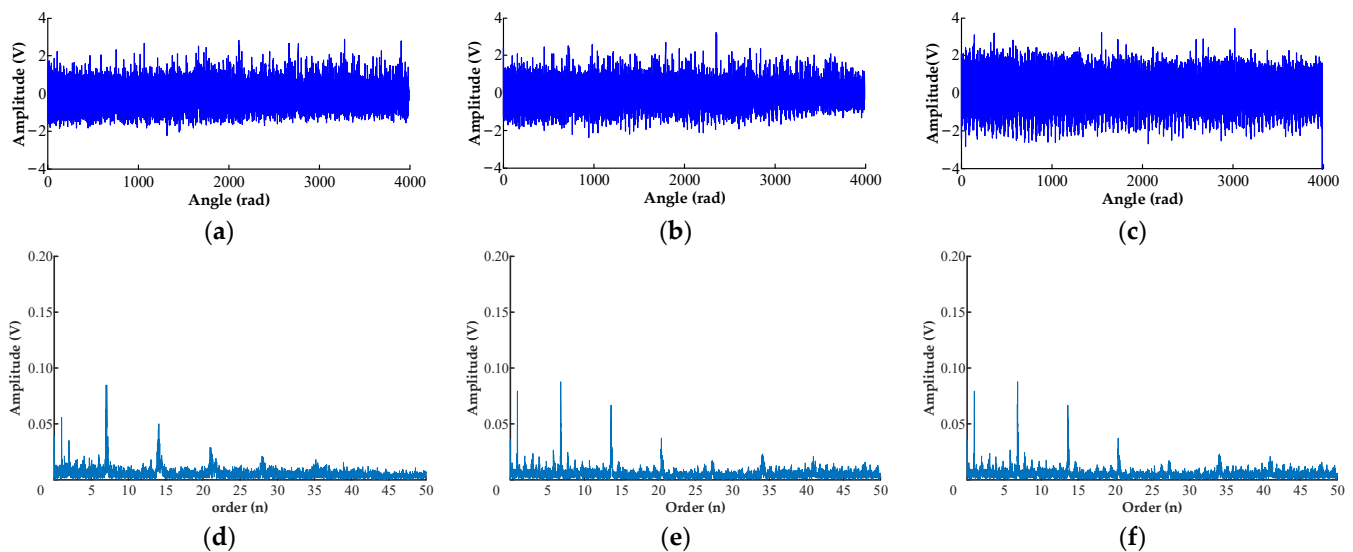
Figure 11. Angular domain vibration signal and order spectrogram under different wear states. (**a**) Angular vibration signal in zero wear state; (**b**) Angular vibration signal in mild wear state; (**c**) Angular vibration signal in moderate wear state; (**d**) Order spectrogram in zero state; (**e**) Order spectrogram in mild state; (**f**) Order spectrogram in moderate state.

Observing the order spectrum of four different states, it can be seen that the amplitude of the order spectrum gradually increases with the continuous increase of wear, and the increase is more pronounced at order 7 and its integral multiples. In the entire order spectrums, the amplitude in the zero-wear state is significantly smaller than that in the worn states. As the wear of the piston pump valve plate increases, the energy of the order band in the corresponding order spectrum also shows a trend of increasing gradually, the more serious the wear degree is, the higher the amplitude of the order spectrum is, and the energy is mainly concentrated in the middle and low order bands.

In the reciprocating process of the piston, with the increasing wear of the valve plate, the force of the oil medium hitting the valve plate becomes larger and larger, and the vibration feedback to the piston pump shell through the parts becomes larger, so the amplitude of the order spectrum can reflect the different degradation states of the piston pump. Through test verification, the order analysis method based on SCT and ACMP can eliminate the influence of variable speed and obtain accurate order spectrums, which conform to reality and have good representativeness.

4. Degradation State Recognition of Piston Pump

4.1. Extraction of Feature Parameters

4.1.1. Characteristic Parameters in Angular Domain

The dimensionless parameters of the signal characteristics are only related to the status of the equipment itself, and they are not sensitive to changes in rotating speed and working conditions. With the continuous increasing wear of the piston pump, the vibration impact transmitted by the shaft to the pump shell will be greater, and the peak index, pulse index, and kurtosis index can reflect the size of the impact energy, so this article selects them as the degradation states' features in the angle domain of the piston pump.

For the angular domain vibration signal $s(l)$ of the piston pump, the data length of the equal angle-interval sampling is L, and the peak index Cf, pulse index If and kurtosis index K_V are defined as follows:

$$Cf = \frac{S_{rms}}{|\overline{S}|}, \ If = \frac{S_{\max}}{|\overline{S}|}, \ K_V = \frac{\beta}{S_{rms}} \tag{15}$$

with

$$S_{rms} = \sqrt{\frac{1}{L}\sum_{l=1}^{L} s^2(l)}, \ S_{\max} = \max(|s(l)|)$$
$$|\overline{S}| = \frac{1}{L}\sum_{l=1}^{L}|s(l)|, \quad \beta = \frac{1}{L}\sum_{l=1}^{L} s^4(l) \tag{16}$$

where S_{rms} is the root mean square value; $S_{\max}$ is the peak value; $|\overline{S}|$ is the absolute mean amplitude; and β is the kurtosis.

Therefore, the degradation characteristic parameter in the angular domain under variable rotational speed is $\mathbf{X} = [Cf, \ If, \ K_V]$.

4.1.2. Characteristic Parameters in Order Domain

At variable rotational speed, the vibration energy intensity of the angular domain signal order spectrum of the axial piston pump has obvious differences in different wear and damage conditions. Therefore, if the order spectrum of the angular domain vibration signal $s(l)(l = 1, 2, 3, \ldots, L)$ is $S_l(m)$, the mean square value of the order spectrum is defined as:

$$Y_1 = \sqrt{\frac{1}{D_{\max}}\sum_{m=1}^{D_{\max}} S^2(m)} \tag{17}$$

where, m is the order data length variable, $m = 1, 2, 3 \ldots D_{\max}$; $D_{\max}$ is the maximum order; and Y_1 is used to weigh the vibrational energy intensity of the entire order spectrum.

In order to better represent the differences in characteristics under different degrees of wear, this paper uses the amplitudes of the 7th, 14th, 21st, and 28th orders of the order spectrum as the characteristic parameters for analysis. In the process of calculating the order spectrum, each signal cannot appear at maximum amplitude exactly at the integer order, so we select the average value of the corresponding order interval as the eigenvalue, as shown in Equation (18).

$$\begin{cases} Y_2 = \frac{\sum S(7 \pm 0.15)}{n} \\ Y_3 = \frac{\sum S(14 \pm 0.15)}{n} \\ Y_4 = \frac{\sum S(21 \pm 0.15)}{n} \\ Y_5 = \frac{\sum S(28 \pm 0.15)}{n} \end{cases} \tag{18}$$

where n is the number of order spectral data in the interval.

Finally, the order domain degradation characteristic selection of the signal at variable rotational speed is $\mathbf{Y} = [Y_1, Y_2, Y_3, Y_4, Y_5]$.

4.2. Pattern Recognition of Degradation States

4.2.1. Parameters Optimization of Model

The vibration signals of the piston pump at variable rotating speeds under four degraded states are collected, and the ACMP, SCT and order analysis are combined to eliminate the spectral ambiguity caused by the change of speed, so as to obtain the reconstructed signal in the angular domain and extract the degradation characteristic parameters of each group of signals. The first five sets of characteristic parameters of the piston pump in the four degraded states are listed, as shown in Table 3.

Table 3. Test samples and corresponding target feature parameters.

Degradation States	Degradation Feature Parameters of The Samples								Label
	Cf	*If*	K_V	Y_1	Y_2	Y_3	Y_4	Y_5	
zero state	17.5143	254.8358	34.3117	0.2943	0.0847	0.0500	0.0298	0.0212	1
	17.0268	259.6160	30.4657	0.3278	0.0865	0.0769	0.0265	0.0208	1
	17.6276	241.1742	37.9160	0.2407	0.0698	0.0532	0.0367	0.0174	1
	17.2683	261.2015	32.2628	0.3097	0.0975	0.0671	0.0111	0.0367	1
	17.4314	259.1114	33.1784	0.2991	0.0967	0.0954	0.0104	0.0079	1
mild wear	12.9107	195.3979	24.4784	0.3316	0.0877	0.0667	0.0374	0.0172	2
	12.5098	211.0776	22.1202	0.3580	0.0876	0.0643	0.0486	0.0123	2
	13.0235	189.0926	26.0609	0.3297	0.0799	0.0793	0.0376	0.0109	2
	12.7630	193.2093	24.5660	0.3436	0.0707	0.0621	0.0291	0.0215	2
	12.8913	194.7280	24.4312	0.3371	0.0782	0.0598	0.0359	0.0188	2
moderate wear	11.1787	228.7917	14.0893	0.6974	0.1482	0.1591	0.0298	0.0635	3
	10.7528	249.2090	12.2644	0.8239	0.1276	0.1689	0.1055	0.0987	3
	11.5477	210.8446	15.8551	0.6122	0.2690	0.1542	0.0965	0.0543	3
	11.0072	241.7709	13.0180	0.7909	0.1098	0.1778	0.1478	0.1214	3
	11.1132	228.4637	14.0665	0.7023	0.1725	0.1161	0.0571	0.0513	3
severe wear	7.5224	247.6851	6.5347	1.0712	0.3681	0.2663	0.1156	0.1074	4
	7.2278	271.0355	6.2371	1.7685	0.2861	0.3791	0.7120	0.1899	4
	7.7621	229.8977	6.6778	0.9976	0.5876	0.2003	0.1485	0.2358	4
	7.3447	258.1544	6.3316	1.2907	0.4760	0.3123	0.3760	0.1010	4
	7.4752	247.9941	6.4727	1.1439	0.5523	0.1796	0.1147	0.2259	4

In this table, $Cf, If, K_V, Y_1, Y_2, Y_3, Y_4, Y_5$ are the input features of the XGBoost model, and the function of label is to distinguish the characteristic parameters of different states more intuitively. It can be seen from the table that there are obvious differences in the same features between different states. For example, the peak index gradually decreases with the increase of wear, and the features related to the order domain gradually become larger with the increase of wear. Similarly, there are also obvious differences between different features of the same state. It can also be seen from the table that there is little difference in the same characteristics of the same state.

In order to improve the performance of the model, the parameters of XGBoost need to be adjusted. In this paper, three parameters are mainly discussed and analyzed: the number of trees, the max depth of tree and the min child weight. Based on fixing other parameters, we change the number of trees, the max depth of the tree and the min child weight to find the optimal parameters, so the overfitting of the model can be avoided and the accuracy of the model can be improved. Since the max depth of the tree and the number of trees affect each other, if the parameters are optimized in turn, it will only fall into the disadvantages of low efficiency and local optimization, and the amount of data in this paper is small, so the grid algorithm can be used to select the optimal parameters for the max depth of the tree and the min child weight at the same time. The results are shown in Figure 12.

As can be seen from the above figure, when the max depth of the tree is 3 and the min child weight is 1, the accuracy of state recognition is the highest. Then, these two parameters are fixed, and the number of decision trees is selected by the logarithmic loss algorithm [34], and then the probability output of the XGBoost classifier is evaluated. The logarithmic loss function is defined as:

$$\sigma = -\frac{1}{N}\sum_{i=1}^{N}\sum_{j=1}^{M}y_{ij}\log(p_{ij}) \tag{19}$$

where N is the input sample size; M is the number of categories; y_{ij} is the true category of the input data points; and p_{ij} is the probability that the i-th data point predicted by the XGBoost classifier belongs to the j-th class. The result is shown in Figure 13.
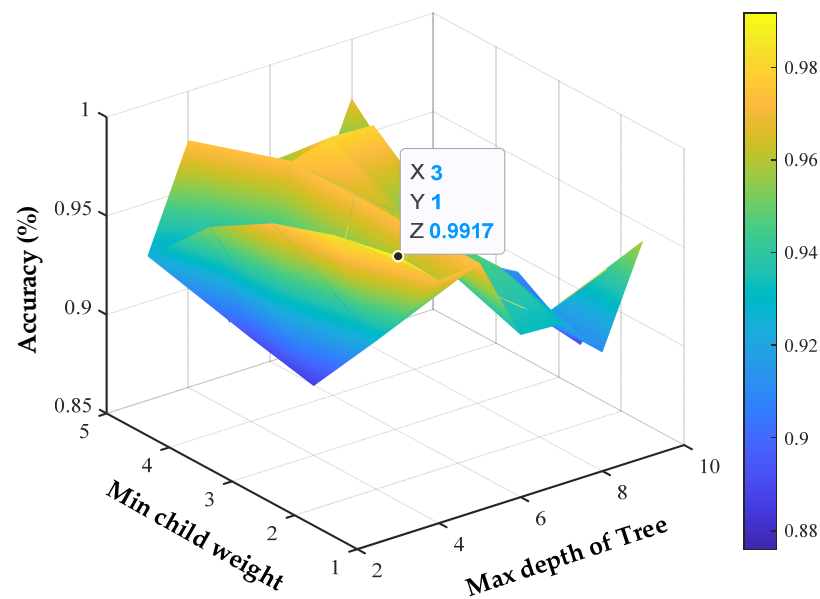
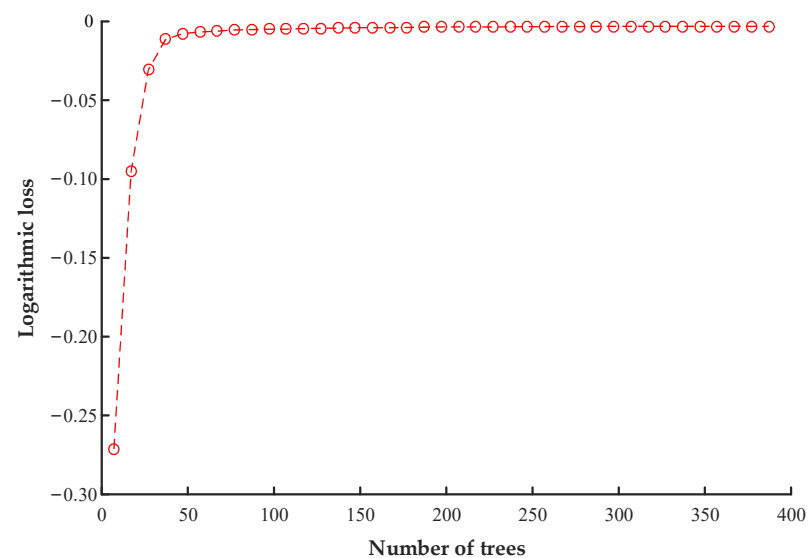**Figure 12.** The parameters selection of the model.

Figure 13. Number selection of trees.

The closer the logarithmic loss value is to zero, the more accurate the XGBoost classifier is. From Figure 13, when the number of trees is 54, the logarithmic loss value is -0.0061, which is the largest value, so it is determined that the number of trees is 54. Through the selection calculation, the optimal parameters of the XGBoost model are shown in Table 4, and the remaining parameters are set to default values.

Table 4. Parameters for XGBoost.

Parameters	Numerical Value
max depth	3
min child weight	1
number of trees	54
learning rate	0.1
objective	multi: softmax
number of categories	4

4.2.2. Recognition Results and Analysis

In order to better verify the efficiency and correctness of this method, K-fold cross validation [35] is used to calculate the recognition accuracy of the XGBoost model, and the average of the multiple test accuracy rates is used as the final test accuracy.

Moreover, the method adopted in this paper is also compared with ANN, SVM, and gradient boosting decision Tree (GBDT) shown in Table 5. It is found that, when the number of hidden layer neurons of ANN is 12, the effect is better; while the kernel function of SVM is RBF, the penalty coefficient is 4, and gamma is 0.1. By adjusting and optimizing the parameters of GBDT, *n* estimators = 20, max depth = 3, and min samples split (the minimum number of samples needed when the internal nodes are divided again) = 10.

Table 5. Comparison of degradation state recognition results.

Classification Method	Average Recognition Accuracy	Mean Decision Time (s)
ANN	0.963	0.094
SVM	0.989	0.029
GBDT	0.986	0.021
XGBoost	0.991	0.013

The above table shows the average accuracy and mean decision time of multiple state recognition verifications. As can be seen from the table, compared with the other three algorithms, XGBoost has the highest prediction accuracy of 0.991, SVM is next with 0.989, GBDT is 0.986, while ANN has the worst prediction accuracy at 0.963. When the performance of the computer is the same, the mean decision time of XGBoost is less than that of SVM, which is 0.016 s. Compared with the traditional GBDT model, XGBoost adds the control of model complexity and pruning processing, which makes the trained model difficult to overfit, and the calculation time is relatively less. The average recognition rate of GBDT is 0.986, but the mean decision time is lower than that of SVM. ANN needs to iterate repeatedly to get the ideal classification effect, so it has a higher mean decision time than the three other algorithms. In the complex working environment, the vibration data of the piston pump is complex and changeable, so it is necessary to extract a variety of characteristics from the data to carry out an effective diagnosis. Compared with ANN, the parameter optimization calculation of XGBoost is not tedious, and in this experiment, the correct recognition rate of this method can be improved by 2.8%. In the evaluation of the degradation state of the axial piston pump, the XGBoost algorithm can not only ensure high diagnosis accuracy but also reduce calculation time. Therefore, XGBoost has practical application value in the recognition of piston pump degradation patterns.

5. Conclusions

In this paper, the valve plate in different wear states is replaced to simulate the different health states of the piston pump, and by building a degradation testbed, the vibration signals under variable rotating speed are collected to study the degradation state recognition of the axial piston pump. The main conclusions have been drawn:

1. The combined method of ACMP and SCT has obvious advantages in dealing with unstable and high-noise vibration signals at variable rotating speeds. Meanwhile, this method also solves the issue of frequency ambiguity, improves the decomposition efficiency, accurately decomposes the signal mode, and extracts the instantaneous frequency of the axial piston pump.
2. With the increase of the wear degree of the valve plate, the order spectrum amplitude and the order domain energy of the axial piston pump show a clear increasing trend, which proves that the signals processed based on ACMP and SCT conform to the actual situation and have high accuracy.
3. The average recognition accuracy of the valve plate wear state of the axial piston pump based on ACMP, SCT, and XGBoost is 99.1%. Compared with ANN, GBDT, and SVM

algorithms, XGBoost identifies four different wear states better and saves computing time, which highlights the advantages of XGBoost after parameter optimization in pattern recognition.

Author Contributions: All the authors contributed to the original idea and design of the study, to the analysis, to the drafting of the manuscript, reading and approving the final version. Conceptualization, R.G. and Y.L.; methodology, R.G.; validation, R.G., Z.Z. and Y.L.; formal analysis, J.W. and W.C.; resources, J.Z.; data curation, Z.Z.; writing—original draft preparation, Y.L. and Z.Z.; writing—review and editing, R.G. and Y.L.; visualization, Y.L. and W.C.; Software, Z.Z. and W.C.; supervision, J.Z., R.G. and J.W.; project administration, J.Z. and R.G.; funding acquisition, J.Z. and R.G. All authors have read and agreed to the published version of the manuscript.

Informed Consent Statement: Not applicable.

Data Availability Statement: Not applicable.

Conflicts of Interest: The authors declare no conflict of interest.

References

1. Li, L.; Tao, J.-F.; Huang, Y.-X.; Liu, C.-L. Internal leakage detection of hydraulic cylinder based on BP neural network. *Chin. Hydraul. Pneum.* **2017**, 11–15.
2. Wang, F.-S. Development status and test platform construction of high pressure hydraulic components in China. *Constr. Mach. Equip.* **2012**, *43*, 1–7.
3. Yang, T.-L.; Gao, Y.-J.; Kong, X.-D. Fault diagnosis method of piston pump based on wavelet transform. *J. Mech. Eng.* **2005**, *41*, 112–116. [CrossRef]
4. Barszcz, T.; Randall, R.B. Application of spectral kurtosis for detection of a tooth crack in the planetary gear of a wind turbine. *Mech. Syst. Signal Process.* **2009**, *23*, 1352–1365. [CrossRef]
5. Wang, J.; Gao, R.X.; Yan, R. Multi-scale enveloping order spectrogram for rotating machine health diagnosis. *Mech. Syst. Signal Process.* **2014**, *46*, 28–44. [CrossRef]
6. Al-Regib, E.; Ni, J.; Lee, S.-H. Programming spindle speed variation for machine tool chatter suppression. *Int. J. Mach. Tools Manuf.* **2003**, *43*, 1229–1240. [CrossRef]
7. Yang, L.-J.; Zang, B.-H.; Ye, X.-Z. Fast Fourier transform and its applications. *Opto-Electron. Eng.* **2004**, *31* (Suppl. S1), 1–3+7.
8. Ren, Y.; Li, W.; Zhu, Z.; Tong, Z.; Zhou, G. A new fault feature for rolling bearing fault diagnosis under varying speed conditions. *Adv. Mech. Eng.* **2017**, *9*, 1687814017703897. [CrossRef]
9. Liu, D.; Cheng, W.; Wen, W. Rolling bearing fault diagnosis via STFT and improved instantaneous frequency estimation method. *Procedia Manuf.* **2020**, *49*, 166–172. [CrossRef]
10. Wang, L.-H.; Zhao, X.-P.; Wu, J.-X.; Xie, Y.-Y.; Zhang, Y.-H. Motor fault diagnosis based on short-time Fourier transform and convolutional neural network. *Chin. J. Mech. Eng.* **2017**, *30*, 1357–1368. [CrossRef]
11. Wang, J.; Du, G.; Zhu, Z.; Shen, C.; He, Q. Fault diagnosis of rotating machines based on the EMD manifold. *Mech. Syst. Signal Process.* **2020**, *135*, 106443. [CrossRef]
12. Liu, H.; Li, L.; Ma, J. Rolling bearing fault diagnosis based on STFT-deep learning and sound signals. *Shock Vib.* **2016**, *2016*, 6127479. [CrossRef]
13. Saavedra, P.; González, J. New revolution-order transform for analysing non-stationary vibrations. *Insight-Non-Destr. Test. Cond. Monit.* **2005**, *47*, 29–35. [CrossRef]
14. Wang, Y.-R.; Wang, J.; Huang, H.-A. Fault diagnosis of planetary gearboxes based on NLSTFT order tracking under variable speed conditions. *China Mech. Eng.* **2018**, *29*, 1688–1695.
15. Goharrizi, A.Y.; Sepehri, N. A wavelet-based approach to internal seal damage diagnosis in hydraulic actuators. *IEEE Trans. Ind. Electron.* **2009**, *57*, 1755–1763. [CrossRef]
16. Wu, J.; Ke, Z.-X.; Li, N.; Jiang, T.; Huang, W.-G. Fault identification of variable speed gearbox based on wavelet transform. *Coal Mine Mach.* **2018**, *39*, 149–151.
17. Khadem, S.; Rezaee, M. Development of vibration signature analysis using multiwavelet systems. *J. Sound Vib.* **2003**, *261*, 613–633. [CrossRef]

18. Yin, X.-Z.; Yu, S.-L. Time frequency analysis theory and its application. *Mod. Electron. Tech.* **2006**, *29*, 118–120.
19. Wen, L.; Liu, Z.-S.; Ge, Y.-J. Several methods of wavelet denoising. *J. Hefei Univ. Technol. (Nat. Sci.)* **2002**, *25*, 167–172.
20. Si, L.; Wang, Z.; Liu, X.; Tan, C. A sensing identification method for shearer cutting state based on modified multi-scale fuzzy entropy and support vector machine. *Eng. Appl. Artif. Intell.* **2019**, *78*, 86–101. [CrossRef]
21. Ji, Y.; Sun, S. Multitask multiclass support vector machines: Model and experiments. *Pattern Recognit.* **2013**, *46*, 914–924. [CrossRef]
22. Azadeh, A.; Saberi, M.; Kazem, A.; Ebrahimipour, V.; Nourmohammadzadeh, A.; Saberi, Z. A flexible algorithm for fault diagnosis in a centrifugal pump with corrupted data and noise based on ANN and support vector machine with hyper-parameters optimization. *Appl. Soft Comput.* **2013**, *13*, 1478–1485. [CrossRef]
23. Siddiqui, S.A.; Verma, K.; Niazi, K.; Fozdar, M. Real-time monitoring of post-fault scenario for determining generator coherency and transient stability through ANN. *IEEE Trans. Ind. Appl.* **2017**, *54*, 685–692. [CrossRef]
24. Wang, Y.; Liu, N.; Guo, H.; Wang, X. An engine-fault-diagnosis system based on sound intensity analysis and wavelet packet pre-processing neural network. *Eng. Appl. Artif. Intell.* **2020**, *94*, 103765. [CrossRef]
25. Yan, X.; Jia, M. A novel optimized SVM classification algorithm with multi-domain feature and its application to fault diagnosis of rolling bearing. *Neurocomputing* **2018**, *313*, 47–64. [CrossRef]
26. Wang, S.; Xiang, J.; Zhong, Y.; Tang, H. A data indicator-based deep belief networks to detect multiple faults in axial piston pumps. *Mech. Syst. Signal Process.* **2018**, *112*, 154–170. [CrossRef]
27. Zang, X.-S.; Lin, M. Wavelet transform and analysis of intrapulse modulation characteristics of linear frequency modulation signal. *Sci. Technol. Eng.* **2012**, *12*, 9840–9844+9855.
28. Yang, Y.; Peng, Z.; Meng, G.; Zhang, W. Spline-kernelled chirplet transform for the analysis of signals with time-varying frequency and its application. *IEEE Trans. Ind. Electron.* **2011**, *59*, 1612–1621. [CrossRef]
29. Chen, S.; Yang, Y.; Peng, Z.; Dong, X.; Zhang, W.; Meng, G. Adaptive chirp mode pursuit: Algorithm and applications. *Mech. Syst. Signal Process.* **2019**, *116*, 566–584. [CrossRef]
30. Mallat, S.G.; Zhang, Z. Matching pursuits with time-frequency dictionaries. *IEEE Trans. Signal Process.* **1993**, *41*, 3397–3415. [CrossRef]
31. Wan, D.-A.; Sun, D.-J.; Zhao, Y.-J. Synchronous revolution order analysis applicationin fault diagnosis of auto gearbox. *Comput. Meas. Control* **2006**, *14*, 299–300, 332.
32. Wang, L.; Zhou, D.; Zhang, H.; Zhang, W.; Chen, J. Application of relative entropy and gradient boosting decision tree to fault prognosis in electronic circuits. *Symmetry* **2018**, *10*, 495. [CrossRef]
33. Chen, Y.; Wang, X.; Jung, Y.; Abedi, V.; Zand, R.; Bikak, M.; Adibuzzaman, M. Classification of short single-lead electrocardiograms (ECGs) for atrial fibrillation detection using piecewise linear spline and XGBoost. *Physiol. Meas.* **2018**, *39*, 104006. [CrossRef] [PubMed]
34. Hitchcock, J.M. Fractal dimension and logarithmic loss unpredictability. *Theor. Comput. Sci.* **2003**, *304*, 431–441. [CrossRef]
35. Rodriguez, J.D.; Perez, A.; Lozano, J.A. Sensitivity analysis of k-fold cross validation in prediction error estimation. *IEEE Trans. Pattern Anal. Mach. Intell.* **2009**, *32*, 569–575. [CrossRef] [PubMed]